Composites Science and Technology 79 (2013) 1–7

Contents lists available at SciVerse ScienceDirect

Composites Science and Technology

journal homepage: www.elsevier.com/locate/compscitech

Full recovery of fiber/matrix interfacial bond strength using a microencapsulated solvent-based healing system

A.R. Jones [a], B.J. Blaiszik [b,d], S.R. White [b,c], N.R. Sottos [b,d,*]

[a] Department of Mechanical Science and Engineering, University of Illinois at Urbana-Champaign, Urbana, IL 61801, United States
[b] Beckman Institute of Science and Technology, University of Illinois at Urbana-Champaign, Urbana, IL 61801, United States
[c] Department of Aerospace Engineering, University of Illinois at Urbana-Champaign, Urbana, IL 61801, United States
[d] Department of Material Science and Engineering, University of Illinois at Urbana-Champaign, Urbana, IL 61801, United States

ARTICLE INFO

Article history:
Received 9 November 2012
Received in revised form 11 January 2013
Accepted 6 February 2013
Available online 18 February 2013

Keywords:
Self-healing
A. Polymer–matrix composites (PMCs)
B. Fiber/matrix bond
A. Glass fibers

ABSTRACT

Full recovery of interfacial bond strength after complete fiber/matrix debonding is achieved with a microencapsulated solvent-based healing chemistry. The surface of a glass fiber is functionalized with microcapsules containing varying concentrations of reactive epoxy resin and ethyl phenylacetate (EPA) solvent. Microbond specimens consisting of a single fiber and a microdroplet of epoxy are tested, and the interfacial shear strengths (IFSSs) during the initial (virgin) debonding and subsequent healing events are measured. Debonding of the fiber/matrix interface ruptures the capsules, releasing resin and solvent into the crack plane. The solvent swells the matrix, initiating transport of residual amine functionality for further curing with the epoxy resin delivered to the crack plane. Using a resin-solvent ratio of 3:97, we achieve a maximum of 100% IFSS recovery–a significant enhancement over prior work that reported 44% average recovery of IFSS with microencapsulated dicyclopentadiene (DCPD) monomer and Grubbs' 1st Generation catalyst healing agents. The effects of capsule coverage, resin-solvent ratio, and capsule size on recovery of IFSS are also determined, providing guidelines for integration of this healing system into high fiber volume fraction structural composites. High healing efficiencies were achieved with capsules as small as 0.6 μm average diameter.

1. Introduction

Fiber-reinforced composites are susceptible to complex damage modes that span multiple length scales and include fiber debonding, fiber pull-out, interlaminar matrix cracking, delamination, and matrix deformation [1]. In nature, biological composites respond to damage through sophisticated, autonomic healing and regenerative mechanisms. Self-healing response in both bulk polymers and fiber-reinforced composites has been achieved through a range of approaches [2], including embedding healing-agent-filled microcapsules [3–24] or hollow fibers [25–27], incorporating pervasive vascular networks [28–34], or by exploiting intrinsic self-healing mechanisms in the polymer architecture [35–40]. For microcapsule-based techniques, mechanical damage triggers autonomic delivery of healing agents to the crack plane, which then polymerize upon mixing. White et al. [3] first demonstrated a capsule-catalyst healing chemistry in which an encapsulated monomer (DCPD) reacts with an embedded catalyst (Grubbs 1st Generation) to form poly (DCPD) upon ring-opening-metathesis-polymerization (ROMP). Other successful self-healing systems include dual capsules for two-part reactions [15–19], a combination of phase separation and encapsulation to isolate components [20,21], or specific to this work, utilizing latent functionality in the matrix to react with a healing agent delivered from a single capsule [22–24].

Fiber/matrix debonding in advanced composites has recently become a focus of self-healing research [7,13,40]. Debonding of the matrix from the reinforcement in composite materials prevents efficient load transfer and causes a significant loss in stiffness and strength [1]. Damage that initiates at the fiber/matrix interface can coalesce to form larger scale damage in the composite, particularly for the case of fatigue loading. In prior work, capsule-based strategies were used to heal microcracking and delamination damage in woven fiber-reinforced composites [5,11,12,41]. The microcapsules in these studies were relatively large (20–100 μm diameter) in order to deliver sufficient healing agent to fill the damage volume. Since the crack separation associated with fiber/matrix interfacial debonding is minimal, capsule size and the amount of healing agent delivered can be significantly reduced. Furthermore, the integration of smaller capsules at the fiber/matrix interface sequesters the healing agent specifically at the location of damage.

* Corresponding author at: Department of Materials Science 1304 W. Green St. Urbana, IL 61801, United States. Tel.: +1 217 333 1041.
E-mail address: n-sottos@ilinois.edu (N.R. Sottos).

0266-3538/$ - see front matter © 2013 Elsevier Ltd. All rights reserved.
http://dx.doi.org/10.1016/j.compscitech.2013.02.007

Multiple methods exist to characterize the interfacial bond between the fiber and matrix including: single fiber microbond and pull out [42,43], fragmentation [44–48], or pushout tests [49–53]. Recently, Blaiszik et al. [13] demonstrated a 44% recovery of interfacial shear strength (IFSS) in a single fiber microbond testing method. Standard glass fibers were functionalized with ca. 1.5 μm capsules containing DCPD monomer [9] and Grubbs' 1st Generation catalyst. Upon debonding of the interface, the DCPD capsules rupture, releasing the monomer to the fiber surface where exposure to the catalyst initiated polymerization of the healing agent and repair of the fiber/matrix bond. Peterson et al. [40] also demonstrated a successful remendable approach to heal interfacial damage. Maliemide-functionalized single glass fibers in a furan-functionalized epoxy were able to recover an average of 41% recovery after heat treatment.

In this paper, we adopt a single capsule, solvent-based healing chemistry to heal interfacial damage. This healing chemistry was originally developed for self-healing of bulk polymers by Caruso et al. [22]. Ethyl phenylacetate (EPA) solvent and a reactive resin (EPON 862) are co-encapsulated for simultaneous delivery to the crack plane. We successfully achieve resin-solvent filled capsules less than 1 μm in diameter and functionalize them directly on a glass fiber surface. After rupture, the solvent swells the matrix and increases the probability that residual reactive amines will polymerize the epoxy healing agent in the crack plane. The effects of capsule coverage, resin-solvent ratio, and capsule size on healing efficiency are explored.

2. Materials and methods

2.1. Microcapsule method: materials and characterization

Two types of microcapsules containing EPON 862 (diglycidyl ether of bisphenol-F) dissolved in ethyl phenylacetate (EPA) solvent were prepared by *in situ* polymerization of urea and formaldehyde (UF) using a modified process of Blaiszik et al. [9], summarized in Table 1. Modifications were made to reduce polydispersity and minimize excess surfactant. For both capsule types, the resin-solvent solution was slowly added to a 30 mL aqueous solution of approximately 1.25% ethylene maleic anhydride copolymer (ZeMac 400 EMA), urea, resorcinol and ammonium chloride and allowed to equilibrate for 10 min before sonication. For Type 1 capsules, the resin-solvent ratio of the core was varied from 0 to 50 percent. For Type 2 capsules, hexadecane was co-dissolved in the resin-solvent core to increase hydrophobicity and decrease Ostwald ripening [9]. A 3.2 mm tapered tip of a 750 W Ultrasonic Homogenizer (Cole–Parmer) was placed in the solution for 2 min at 40% intensity with a 0.2 s pulsing parameter under continuous agitation at 800 rpm. Formalin was then added to the encapsulation. The temperature control bath was slowly heated to 55 °C and held constant for 4 h. After the reaction was complete, the capsules were centrifuged and rinsed three times to remove excess surfactant.

Table 1
Parameters for resin-solvent filled capsule types.

Components	Type 1	Type 2
Aqueous phase	15 mL H_2O, 15 mL 2.5% EMA	15 mL H_2O, 15 mL 2.5% EMA
Urea	0.45 g	0.45 g
NH_4Cl	0.1 g	0.1 g
Resorcinol	0.045 g	0.045 g
Formalin	1.2 g	1.2 g
Core	5 mL resin-solvent	4.5 mL resin-solvent
Co-stabilizer	None	2.5 wt.% hexadecane

Microcapsule size distributions were obtained via SEM (FEI/Phillips XL30 ESEM-FEG). All size distributions were determined from a minimum of 200 measurements from multiple images. Thermal stability and overall capsule quality was assessed by thermogravimetric analysis (TGA) in a nitrogen atmosphere at a heating rate of 10 °C/min (Mettler Toledo TGA/DSC 1). Capsules were lyophilized for 3 days before thermal testing.

2.2. Interfacial functionalization

E-glass fibers with a proprietary epoxy-compatible sizing were obtained from Owens Corning (Type 158B-AA-675). The glass fibers had an ultimate tensile strength of 2.0 ± 0.15 GPa and an average diameter of 14.5 ± 0.8 μm [13]. Self-healing (SH) functionalized fibers were coated with resin-solvent microcapsules using a dip-coat technique. A single E-glass fiber was isolated from the tow and dipped once in an aqueous suspension of resin-solvent capsules of known concentration. The capsule coverage, ξ, is defined as the surface area of capsules on the surface of the fiber divided by the surface area of the fiber, or

$$\xi \approx \frac{N\pi r_{cap}^2}{\pi d l_e}, \tag{1}$$

where N is the number of capsules present on the surface of the fiber, r_{cap} is the radius of the capsule, d is the diameter of the fiber, and l_e is the embedded length of the fiber in the microbond specimen. Capsule coverage, ξ, was measured by image analysis of SEM micrographs. Representative SEM images of fibers with varying capsule coverage are shown in Fig. 1. Single fibers were functionalized with several different types of capsules that varied in both diameter and resin-solvent ratio (Table 2).

2.3. Microbond specimen preparation

Microbond specimens consisted of a single glass fiber embedded in an epoxy droplet as shown in Fig. 2. A micropipette was used to apply a bead (180–230 μm in length) of epoxy to either plain (as-received) or functionalized fibers. EPON 828 (diglycidyl ether of bisphenol-A) resin and EPIKURE DETA (diethylenetriamine), an aerospace grade epoxy with high bond strength, was mixed at 12 pph DETA:EPON 828, degassed and allowed to react at room temperature for 2 h before being applied to the fibers.

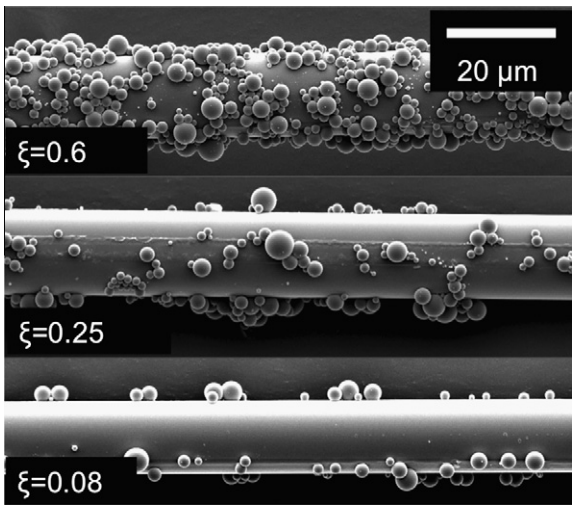

Fig. 1. SEM micrographs of glass fibers (sample type SH1-97) with varying capsule coverage (ξ).

Table 2
Interfacial strengths and healing efficiencies for different specimen types.

Sample type	Core content (862: EPA)	Capsule dia. (μm)	Virgin IFSS (MPa)	Healing efficiency, η	Capsule coverage, ξ	No. of Samples, n
SH1-100	0:100	3.7 ± 1.1	26 ± 1.9	0.72 ± 0.06	0.5	8
SH1-97	3:97	2.1 ± 0.7	33 ± 1.7	0.46 ± 0.07	0.3	14
			29 ± 3.7	0.63 ± 0.08	0.4	8
			28 ± 1.7	0.70 ± 0.06	0.5	13
			23 ± 1.7	0.86 ± 0.07	0.7	16
SH1-90	10:90	1.7 ± 0.8	27 ± 1.5	0.66 ± 0.07	0.5	9
			30 ± 1.6	0.58 ± 0.09	0.3	8
SH1-80	20:80	1.3 ± 0.5	25 ± 2.6	0.76 ± 0.09	0.5	8
			27 ± 2.5	0.63 ± 0.10	0.3	16
SH1-70	30:70	1.2 ± 0.5	33 ± 3.1	0.53 ± 0.08	0.5	9
			28 ± 3.0	0.71 ± 0.09	0.3	11
SH1-50	50:50	1.4 ± 0.6	32 ± 2.4	0.62 ± 0.05	0.5	4
			31 ± 1.6	0.51 ± 0.08	0.3	9
SH2-70	30:70	0.6 ± 0.3	32 ± 3.0	0.34 ± 0.05	0.4	12
			27 ± 3.1	0.50 ± 0.05	0.5	10
			23 ± 1.3	0.60 ± 0.08	0.7	11
SH-DCPD[a]	–	1.6 ± 0.5	27 ± 4.3	0.29 ± 0.06	0.1	11
			26 ± 2.1	0.36 ± 0.06	0.4	14
			21 ± 2.5	0.44 ± 0.05	0.7	18
Control	–	–	32 ± 3.6	0.24 ± 0.04	–	9

[a] The capsule coverages were adapted from Blaiszik et al. [13] for comparison to the present work. Also, a different matrix was used in the prior work which resulted in lower virgin IFSS values.

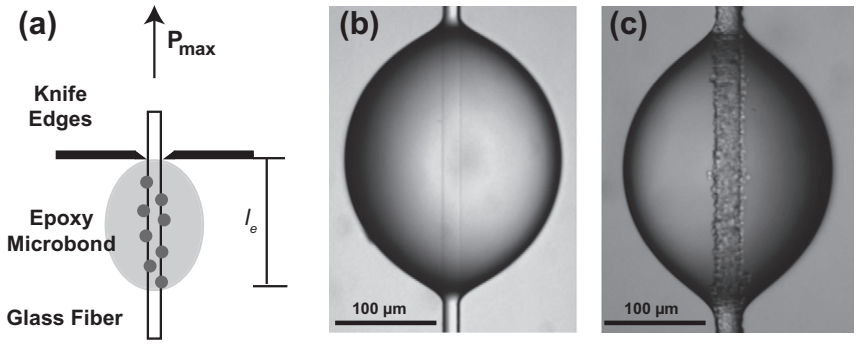

Fig. 2. (a) Schematic of microbond test, (b) optical micrograph of a control and (c) self-healing microbond specimen.

The specimens were cured at room temperature for 24 h and then 24 h at 35 °C.

2.4. Microbond test method

After curing, optical images (Fig. 2) were obtained before testing in order to measure the embedded length (l_e) of each specimen. The samples were tested with a custom-built load frame and imaged simultaneously through a zoom lens to observe interfacial debonding. Samples were loaded in displacement control using a linear actuator (Physik Instrumente) translating at a rate of 0.5 μm/s and controlled through LabView (National Instruments, v10.0). Load was measured with a 150 g load cell (Honeywell Sensotec). Samples were loaded to the maximum force (P_{max}) needed to cause full interfacial debond. After debond, the force dropped quickly and then slowly increased to a frictional plateau value ($P_{friction}$). The sample was then removed from the load frame and allowed to heal for 24 h at room temperature.

The IFSS (τ) was calculated from the peak applied force (P_{max}), the fiber diameter (d), and the embedded length (l_e),

$$\tau = \frac{P_{max}}{\pi d l_e}. \quad (2)$$

The healing efficiency (η) was defined as the ratio of the recovered interfacial shear strength to the original value,

$$\eta = \frac{\tau_{healed}}{\tau_{virgin}} = \frac{P_{max,healed}}{P_{max,virgin}}. \quad (3)$$

In some specimens, Nile Red dye (Sigma–Aldrich) was added to microcapsules (≈0.03 wt.% of resin-solvent core) with a resin-solvent ratio of 3:97 to visualize healing agent delivery *in situ*. Microbond specimens containing the dyed capsules were imaged both before and after interfacial debond on a confocal microscope (Leica SP2).

3. Microcapsule characterization

Representative SEM images of the two types of resin-solvent microcapsules prepared according to Table 1 are shown in Fig. 3 along with corresponding size distributions. Type 1 microcapsules ranged in size from 1.2–3.7 μm in average diameter depending on the ratio of resin to solvent in the core as summarized in Table 2. The average diameter decreased from 3.7 μm for the case of no resin (SH1-100) to approximately 1.2 μm for a resin-solvent ratio of 30:70 (SH1-70). We attribute this decrease in capsule size to the extension of emulsion droplet lifetime provided by the increased viscosity of the resin compared to EPA. The significant decrease in diameter (0.6 ± 0.3 μm) achieved for Type 2 microcapsules (SH2-70) is due to the addition of hexadecane, an ultrahydrophobe, which provided further chemical stabilization to the emulsion (Fig. 3b).

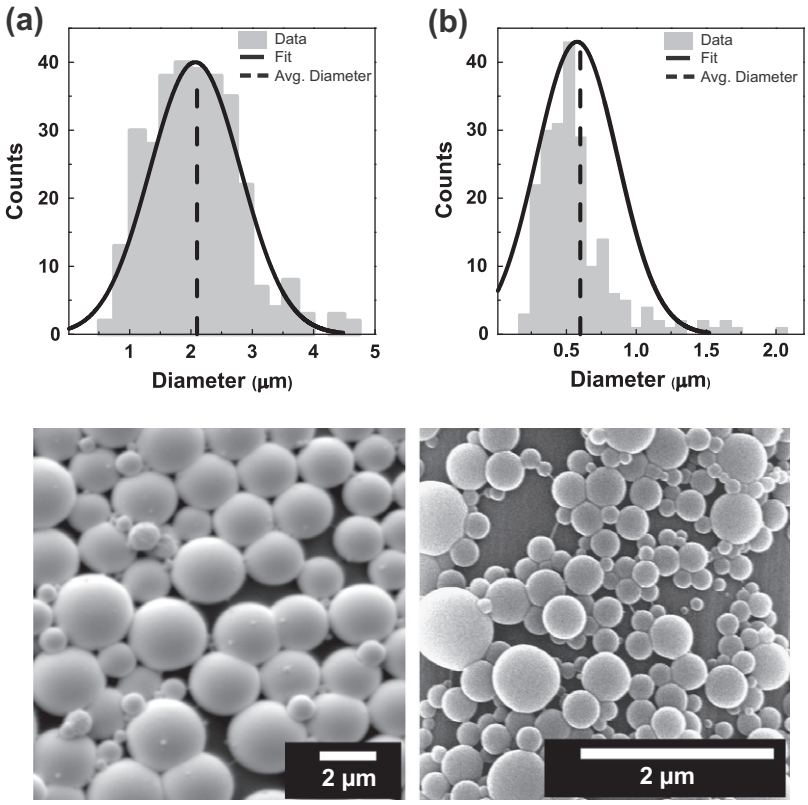

Fig. 3. Typical size distribution and corresponding SEM image for (a) Type 1 capsules with an average diameter of 2.1 ± 0.7 μm (used in SH1-97 samples) and (b) Type 2 capsules with an average diameter of 0.6 ± 0.3 μm (used in SH2-70 samples).

Microcapsule quality was also evaluated by thermal stability testing. Representative TGA traces, presented in Fig. 4, show excellent stability with no significant mass loss before reaching the boiling point of EPA (ca. 225 °C). The precipitous loss of mass at ca. 225 °C corresponds to the mass of EPA encapsulated. The second region of mass loss initiating at ca. 350 °C is associated with the mass of encapsulated EPON 862 and hexadecane (if present). The residual mass corresponds to shell wall material.

4. Recovery of interfacial shear strength

Self-healing of the fiber/matrix interfacial bond was assessed by repeated testing of microbond specimens. A variety of samples were tested with different types of microcapsules functionalized on the glass fibers. A summary of the different sample types, IFSS values, and healing performances is provided in Table 2. Results from Blaiszik et al. [13], which use a DCPD/Grubbs' 1st Generation catalyst healing chemistry and a slightly different matrix of 40 pph EPIKURE 3274:EPON 828, are also included for comparison. A representative load–displacement curve is shown in Fig. 5a for a self-healing specimen (SH1-97). The sample is loaded to 320 mN (P_{max}), before full interfacial debonding, and then quickly reaches the frictional plateau of 70 mN ($P_{friction}$). After 24 h, the sample is re-tested and full recovery of IFSS is achieved for this particular resin-solvent ratio of 3:97. This healing chemistry resulted in the highest healing efficiency of those considered in Table 2. Interestingly, Caruso et al. [22] also found maximum healing at this ratio in bulk polymers. The control specimens, consisting of a plain glass fiber embedded in the same epoxy matrix, only recovered the frictional force (η = 0.24) 24 h after initial testing (Fig. 5b).

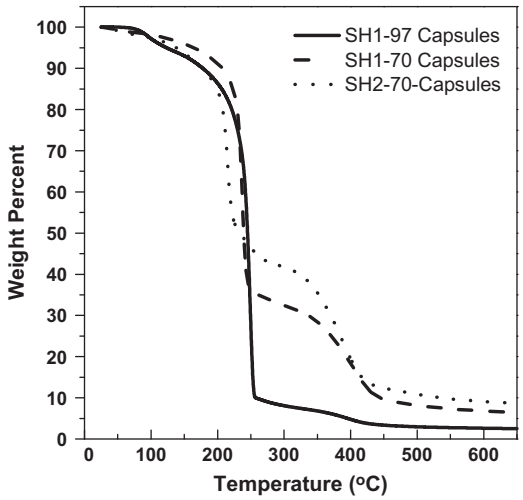

Fig. 4. Representative TGA traces of microcapsules.

In select specimens, the healed region was visualized using confocal fluorescence microscopy. Initially, the capsules were intact with distinct shell walls (Fig. 6a). After loading, a large percentage of the capsules were ruptured and the healing agent was wicked into the crack plane forming regions of healed interface (Fig. 6b). The healed material was not evenly distributed along the fiber/matrix interface, implying healing agent delivery could be further optimized with the goal of reducing the required amount of capsules for maximum healing performance.

4.1. Effect of capsule coverage

Four different capsule coverages were investigated (ξ = 0.3, 0.4, 0.5, 0.7) for the resin-solvent ratio of 3:97 (sample type SH1-97). The effect of capsule coverage on healing efficiency is summarized in Fig. 7 and compared to previous results for the DCPD/Grubbs'

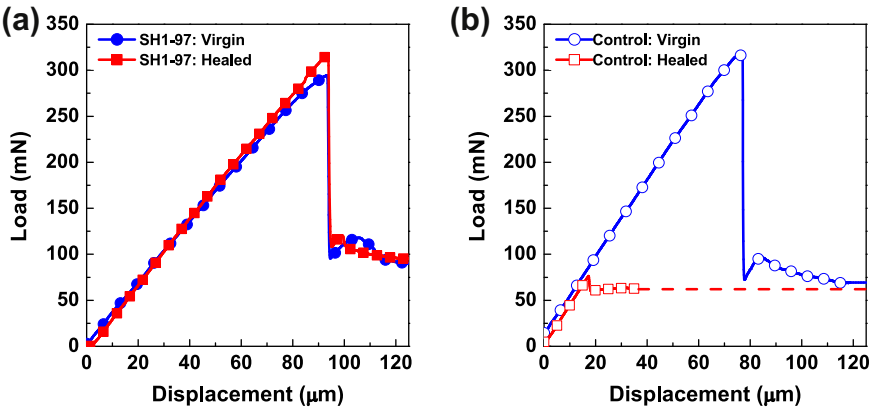

Fig. 5. Representative load–displacement curves for microbond testing of (a) self-healing (SH1-97) specimen with 100% recovery of IFSS and (b) control specimen, which only recovers frictional force.

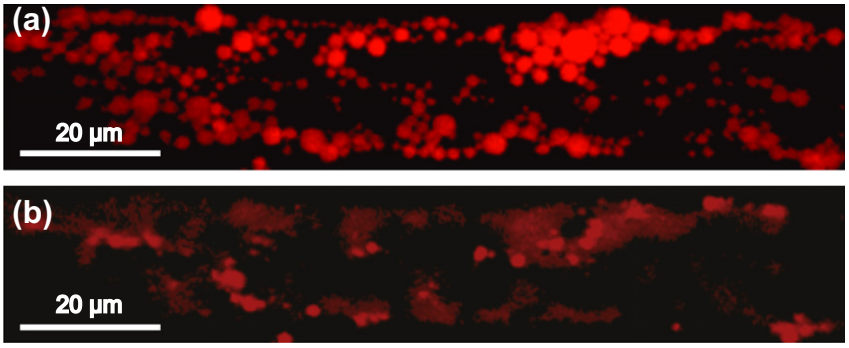

Fig. 6. Confocal fluorescent microscope images of microbond specimens (SH1-97) and a capsule coverage, $\xi = 0.5$: (a) prior to testing and (b) after full debonding.

1st Generation catalyst healing chemistry [13]. Higher capsule coverages resulted in more healing agent delivered to the crack plane and higher healing efficiencies for both healing chemistries. Similar to prior studies [22], the resin-solvent healing chemistry produced higher healing efficiencies than the DCPD/Grubbs' healing chemistry. The increase in healing performance is attributed to improved bonding of an epoxy-based healed film to both the epoxy matrix and glass fiber reinforcement. Additionally, the sensitivity of the Grubbs' catalyst to processing conditions limited healing performance unless additional protection schemes were employed.

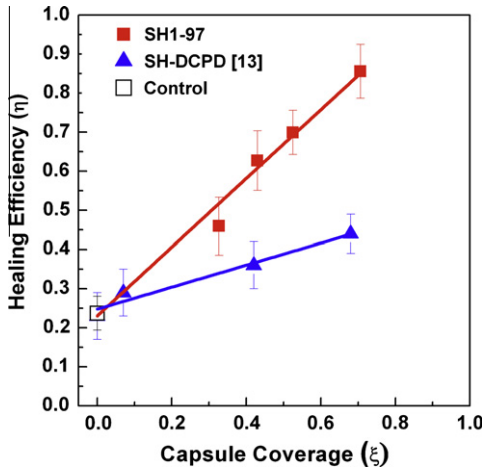

Fig. 7. Healing efficiency as a function of capsule coverage for capsules containing 3:97 resin-solvent ratio (SH1-97) and SH-DCPD adapted from Blaiszik et al. [13].

The effect of interfacial functionalization on healing performance and virgin IFSS is reported in Table 2. At low concentrations, the addition of microcapsules led to modest increases of the virgin IFSS. However, further increases in capsule coverage ($\xi = 0.5$, $\eta = 0.7$) caused a small reduction in IFSS due to less available surface area for the matrix to bond to the fiber. At the highest capsule coverage ($\xi = 0.7$), there was a more significant loss of IFSS, but healing performance was maximized. Interestingly, the IFSS values for submicron Type 2 capsules (SH2-70, capsule diameter ca. 0.6 μm) were similar to those for the larger capsules (SH1-97, capsule diameter ca. 2 μm), indicating the effect of the two microcapsule sizes on IFSS is the same.

4.2. Effect of resin-solvent ratio and capsule size

Microcapsules were prepared over a range of resin-solvent ratios as listed in Table 2. Microbond specimens functionalized with these capsules were tested and healing efficiency was calculated as a function of the volume of resin (EPON 862) delivered to the crack plane (Fig. 8). The volume (V) delivered was calculated from

$$V = \frac{4}{3}\pi r_{cap}\xi d l_e \phi, \tag{4}$$

where r_{cap} is the radius of the capsule, ξ is the capsule coverage, d is the diameter of the fiber, l_e is the embedded length of the fiber, and ϕ is the percentage of resin encapsulated. Eq. 4 assumes that all capsules rupture and as such represents a theoretical upper limit. For samples made with Type 1 capsules, we found a critical volume of resin (ca. 200 μm^3) was necessary for high healing efficiencies. Healing efficiency was maximum at 300 μm^3 using SH1-97 capsules with $\xi = 0.7$. Increasing the volume of resin delivered did not further

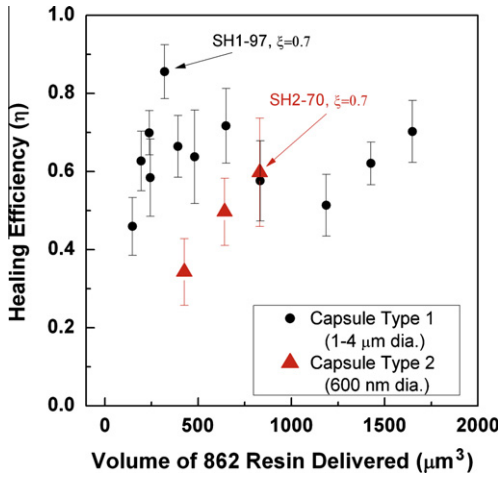

Fig. 8. The performance of Type 2 submicron capsules is highlighted in comparison to Type 1 capsules.

increase healing efficiency. A similar effect was noted by Caruso et al. [22] for bulk epoxy in which it was hypothesized that an excess of resin in the crack plane leads to incomplete cure by residual amines in the matrix.

For healing experiments with smaller Type 2 capsules, a resin-solvent ratio of 30:70 was selected in order to increase the volume of resin delivered to the crack plane. Due to the reduction in capsule diameter, and therefore healing agent delivered, a higher percentage of encapsulated resin is necessary in order to reach the critical volume of resin indicated in Fig. 8. Microbond specimens functionalized with Type 2 capsules were tested and the average healing efficiencies recorded. The results are plotted with the values obtained from larger Type 1 capsules in Fig. 8. A maximum of 83% healing efficiency was obtained using 0.6 μm submicron capsules for select samples at a capsule coverage of $\xi = 0.7$. In general for Type 2 capsules, a greater volume of EPON 862 is required to attain high healing efficiencies (Fig. 8). The observed decrease in performance, when compared to the larger capsules, is likely due to residual hexadecane in the crack plane and a lower core to shell ratio for similar capsule coverages.

5. Conclusions

Nearly full recovery of interfacial shear strength for a glass/epoxy composite was achieved with a single capsule, resin-solvent self-healing chemistry. With increasing capsule coverage, higher healing efficiencies were achieved with only a small decrease in the IFSS. The effect of the resin-solvent ratio was also examined with respect to the volume of EPON 862 delivered. A critical volume of EPON 862 resin (ca. 300 μm^3) was required for maximum recovery of IFSS. Above this critical volume, however, the healing efficiency did not increase further. This critical volume of resin was used to prepare submicron capsules (0.6 μm diameter) using a resin-solvent ratio of 30:70, in which a maximum of 83% recovery of IFSS was achieved. In future studies, we envision these key parameters will enable application of this healing approach to other fiber/epoxy systems.

Acknowledgements

This work was supported by the Air Force Office of Scientific Research (Grant No. FA9550-10-1-0126). The authors would like to acknowledge S. Robinson and M. Bee from the Imaging Technology Group at the Beckman Institute, University of Illinois Urbana-Champaign for their aid in electron and confocal microscopy. The authors would also like to thank Dr. Jericho Moll, Dr. Amit Patel, and Dr. Henghua Jin for helpful discussions.

References

[1] Cantwell WJ, Morton J. The significance of damage and defects and their detection in composite materials: a review. J Strain Anal Eng Des 1992;27(1):29–42. http://dx.doi.org/10.1243/03093247V271029.
[2] Blaiszik B, Kramer S, Olugebefola S, Moore J, Sottos N, White S. Self-healing polymers and composites. Ann Rev Mater Res 2010;40(1):179–211. http://dx.doi.org/10.1146/annurev-matsci-070909-104532.
[3] White SR, Sottos NR, Geubelle PH, Moore JS, Kessler MR, Sriram SR, et al. Autonomic healing of polymer composites. Nature 2001;409(6822):794–7. http://dx.doi.org/10.1038/35057232.
[4] Brown E, Sottos N, White S. Fracture testing of a self-healing polymer composite. Exp Mech 2002;42(4):372–9. http://dx.doi.org/10.1007/BF02412141.
[5] Kessler M, Sottos N, White S. Self-healing structural composite materials. Compos Part A: Appl Sci Manuf 2003;34(8):743–53. http://dx.doi.org/10.1016/S1359-835X(03)00138-6.
[6] Brown E, White S, Sottos N. Retardation and repair of fatigue cracks in a microcapsule toughened epoxy composite Part II: In situ self-healing. Compos Sci Technol 2005;65(15–16):2474–80. http://dx.doi.org/10.1016/j.compscitech.2005.04.053.
[7] Sanada K, Yasuda I, Shindo Y. Transverse tensile strength of unidirectional fibre-reinforced polymers and self-healing of interfacial debonding. Plast Rubber Compos 2006;35(2):67–72. http://dx.doi.org/10.1179/174328906X79914.
[8] Rule JD, Sottos NR, White SR. Effect of microcapsule size on the performance of self-healing polymers. Polymer 2007;48(12):3520–9. http://dx.doi.org/10.1016/j.polymer.2007.04.008.
[9] Blaiszik B, Sottos N, White S. Nanocapsules for self-healing materials. Compos Sci Technol 2008;68(3–4):978–86. http://dx.doi.org/10.1016/j.compscitech.2007.07.021.
[10] Kirkby EL, Rule JD, Michaud VJ, Sottos NR, White SR, Mnson JAE. Embedded shape-memory alloy wires for improved performance of self-healing polymers. Adv Funct Mater 2008;18(15):2253–60. http://dx.doi.org/10.1002/adfm.200701208.
[11] Moll JL, White SR, Sottos NR. A self-sealing fiber-reinforced composite. J Compos Mater 2010;44(22):2573–85. http://dx.doi.org/10.1177/0021998309356605.
[12] Patel AJ, Sottos NR, Wetzel ED, White SR. Autonomic healing of low-velocity impact damage in fiber-reinforced composites. Compos Part A: Appl Sci Manuf 2010;41(3):360–8. http://dx.doi.org/10.1016/j.compositesa.2009.11.002.
[13] Blaiszik BJ, Baginska M, White SR, Sottos NR. Autonomic recovery of fiber/matrix interfacial bond strength in a model composite. Adv Funct Mater 2010;20(20):3547–54. http://dx.doi.org/10.1002/adfm.201000798.
[14] Yin T, Zhou L, Rong MZ, Zhang MQ. Self-healing woven glass fabric/epoxy composites with the healant consisting of micro-encapsulated epoxy and latent curing agent. Smart Mater Struct 2008;17(1). http://dx.doi.org/10.1088/0964-1726/17/01/015019.
[15] Xiao DS, Yuan YC, Rong MZ, Zhang MQ. Self-healing epoxy based on cationic chain polymerization. Polymer 2009;50(13):2967–75. 16/j.polymer.2009.04.029.
[16] Yuan YC, Rong MZ, Zhang MQ, Chen J, Yang GC, Li XM. Self-healing polymeric materials using Epoxy/Mercaptan as the healant. Macromolecules 2008;41(14):5197–202. http://dx.doi.org/10.1021/ma800028d.
[17] Keller MW, White SR, Sottos NR. A self-healing poly(dimethyl siloxane) elastomer. Adv Funct Mater 2007;17(14):2399–404. http://dx.doi.org/10.1002/adfm.200700086.
[18] Beiermann BA, Keller MW, Sottos NR. Self-healing flexible laminates for resealing of puncture damage. Smart Mater Struct 2009;18(8):085001. http://dx.doi.org/10.1088/0964-1726/18/8/085001.
[19] Jin H, Mangun CL, Stradley DS, Moore JS, Sottos NR, White SR. Self-healing thermoset using encapsulated epoxy-amine healing chemistry. Polymer 2012;53(2):581–7. http://dx.doi.org/10.1016/j. polymer.2011.12.005.
[20] Cho SH, Andersson HM, White SR, Sottos NR, Braun PV. Polydimethylsiloxane-based self-healing materials. Adv Mater 2006;18(8):997–1000. http://dx.doi.org/10.1002/adma.200501814.
[21] Cho SH, White SR, Braun PV. Self-healing polymer coatings. Adv Mater 2009;21(6):645–9. http://dx.doi.org/10.1002/adma.200802008.
[22] Caruso MM, Blaiszik BJ, White SR, Sottos NR, Moore JS. Full recovery of fracture toughness using a nontoxic solvent-based self-healing system. Adv Funct Mater 2008;18(13):1898–904. http://dx.doi.org/10.1002/adfm.200800300.
[23] Blaiszik B, Caruso M, McIlroy D, Moore J, White S, Sottos N. Microcapsules filled with reactive solutions for self-healing materials. Polymer 2009;50(4):990–7. http://dx.doi.org/10.1016/j.polymer.2008.12.040.
[24] Zako M, Takano N. Intelligent material systems using epoxy particles to repair microcracks and delamination damage in GFRP. J Intel Mater Syst Struct 1999;10(10):836–41. http://dx.doi.org/10.1106/YEIH-QUDH-FC7W-4QFM.
[25] Trask R, Williams G, Bond I. Bioinspired self-healing of advanced composite structures using hollow glass fibres. J Roy Soc Interf 2007;4(13):363–71. http://dx.doi.org/10.1098/rsif.2006.0194.

[26] Williams G, Trask R, Bond I. A self-healing carbon fibre reinforced polymer for aerospace applications. Compos Part A: Appl Sci Manuf 2007;38(6):1525–32. doi:16/j.compositesa.2007.01.013.
[27] Pang J, Bond I. 'Bleeding composites'–damage detection and self-repair using a biomimetic approach. Compos Part A: Appl Sci Manuf 2005;36(2):183–8. doi:16/j.compositesa.2004.06.016.
[28] Toohey KS, Sottos NR, Lewis JA, Moore JS, White SR. Self-healing materials with microvascular networks. Nat Mater 2007;6(8):581–5. http://dx.doi.org/10.1038/nmat1934.
[29] Hansen CJ, Wu W, Toohey KS, Sottos NR, White SR, Lewis JA. Self-healing materials with interpenetrating microvascular networks. Adv Mater 2009;21(41):4143–7. http://dx.doi.org/10.1002/adma.200900588.
[30] Hamilton AR, Sottos NR, White SR. Self-healing of internal damage in synthetic vascular materials. Adv Mater 2010;22(45):5159–63. http://dx.doi.org/10.1002/adma.201002561.
[31] Hamilton AR, Sottos NR, White SR. Pressurized vascular systems for self-healing materials. J Roy Soc Interf 2011;9(70):1020–8. http://dx.doi.org/10.1098/rsif.2011.0508.
[32] Hansen CJ, White SR, Sottos NR, Lewis JA. Accelerated self-healing via ternary interpenetrating microvascular networks. Adv Funct Mater 2011;21(22):4320–6. http://dx.doi.org/10.1002/adfm.201101553.
[33] Williams H, Trask R, Bond I. Self-healing sandwich panels: restoration of compressive strength after impact. Compos Sci Technol 2008;68(15–16):3171–7. http://dx.doi.org/10.1016/j.compscitech.2008.07.016.
[34] Esser-Kahn AP, Thakre PR, Dong H, Patrick JF, Vlasko-Vlasov VK, Sottos NR, et al. Three-dimensional microvascular fiber-reinforced composites. Adv Mater 2011;23(32):3654–8. http://dx.doi.org/10.1002/adma.201100933.
[35] Chen X, Dam MA, Ono K, Mal A, Shen H, Nutt SR, et al. A thermally re-mendable cross-linked polymeric material. Science 2002;295(5560):1698–702. http://dx.doi.org/10.1126/science.1065879.
[36] Park JS, Takahashi K, Guo Z, Wang Y, Bolanos E, Hamann-Schaffner C, et al. Towards development of a self-healing composite using a mendable polymer and resistive heating. J Compos Mater 2008;42(26):2869–81. http://dx.doi.org/10.1177/0021998308097280.
[37] Kalista SJ, Ward TC, Oyetunji Z. Self-healing of poly(ethylene-co-methacrylic acid) copolymers following projectile puncture. Mech Adv Mater Struct 2007;14(5):391–7. http://dx.doi.org/10.1080/15376490701298819.
[38] Varley RJ, van der Zwaag S. Towards an understanding of thermally activated self-healing of an ionomer system during ballistic penetration. Acta Mater 2008;56(19):5737–50. http://dx.doi.org/10.1016/j.actamat.2008.08.008.
[39] Cordier P, Tournilhac F, Soulie-Ziakovic C, Leibler L. Self-healing and thermoreversible rubber from supramolecular assembly. Nature 2008;451(7181):977–80. http://dx.doi.org/10.1038/nature06669.
[40] Peterson AM, Jensen RE, Palmese GR. Thermoreversible and remendable glasspolymer interface for fiber-reinforced composites. Compos Sci Technol 2011;71(5):586–92. http://dx.doi.org/10.1016/j.compscitech.2010.11.022.
[41] Moll JL, White SR, Sottos NR. Self-healing of mechanical damage in a fully cured structural composite. Composites Science and Technology; Accepted for publication. http://dx.doi.org/10.1016/j.compscitech.2013.02.006.
[42] Zhandarov S, Gorbatkina Y, Mäder E. Adhesional pressure as a criterion for interfacial failure in fibrous microcomposites and its determination using a microbond test. Compos Sci Technol 2006;66(15):2610–28. http://dx.doi.org/10.1016/j.compscitech.2006.03.023.
[43] Zhandarov S, Mäder E. Peak force as function of the embedded length in pull-out and microbond tests: effect of specimen geometry. J Adhes Sci Technol 2005;19(10):817–55. http://dx.doi.org/10.1163/1568561054929937.
[44] Yilmaz YI. Analyzing single fiber fragmentation test data by using stress transfer model. J Compos Mater 2002;36(5):537–51. http://dx.doi.org/10.1177/0021998302036005465.
[45] Wagner HD, Nairn JA, Detassis M. Toughness of interfaces from initial fiber–matrix debonding in a single fiber composite fragmentation test. Appl Compos Mater 1995;2(2):107–17. http://dx.doi.org/10.1007/BF00569253.
[46] Kim BW, Nairn JA. Observations of fiber fracture and interfacial debonding phenomena using the fragmentation test in single fiber composites. J Compos Mater 2002;36(15):1825–58. http://dx.doi.org/10.1177/0021998302036015243.
[47] Gong XJ, Arthur JA, Penn LS. Strain rate effect in the single-fiber fragmentation test. Polym Compos 2001;22(3):349–60. http://dx.doi.org/10.1002/pc.10543.
[48] Wadsworth NJ, Spilling I. Load transfer from broken fibres in composite materials. J Phys D: Appl Phys 1968;1(8):1049–58. http://dx.doi.org/10.1088/0022-3727/1/8/312.
[49] Lin G, Geubelle P, Sottos N. Simulation of fiber debonding with friction in a model composite pushout test. Int J Solids Struct 2001;38(46–47):8547–62. http://dx.doi.org/10.1016/S0020-7683(01)00085-3.
[50] Liang C, Hutchinson J. Mechanics of the fiber pushout test. Mech Mater 1993;14(3):207–21. http://dx.doi.org/10.1016/0167-6636(93)90067-2.
[51] Cordes RD, Daniel IM. Determination of interfacial properties from observations of progressive fiber debonding and pullout. Compos Eng 1995;5(6):633–48. http://dx.doi.org/10.1016/0961-9526(95)00009-C.
[52] Bechel V, Sottos N. Application of debond length measurements to examine the mechanics of fiber pushout. J Mech Phys Solids 1998;46(9):1675–97. http://dx.doi.org/10.1016/S0022-5096(97)00040-9.
[53] Bechel VT, Sottos NR. High temperature fiber pushout of pristine and transversely fatigued SiC/Ti-6-4. J Mater Sci 1999;34(14):3471–8. http://dx.doi.org/10.1023/A:1004657804853.